DESIGN AND TESTING OF AN IMPACT SENSOR USING TWO CROSSED POLYVINYLIDENE FLUORIDE (PVDF) FILMS

Y. Sun, R. Cao, Z. Lu, X. Nie, Z. K. Li, Y. H. Yu,
H. P. Tian, X. Q. Qian, J. P. Wang

HIGHLIGHTS

- An impact sensor with two orthogonal layers of PVDF films was designed.
- Collision tests were performed to measure the sensor's performance on a self-developed test bench.
- The sensor has a very high detection efficiency and can identify simultaneous impacts.

ABSTRACT. *Impact sensors are widely used to detect grain losses in harvesters. Using polyvinylidene fluoride (PVDF) films as sensing elements is a promising way to improve sensor performance due to their high sensitivity, stability, and flexibility. However, the overlap of collision signals significantly reduces the accuracy of a sensor. To solve this problem, a novel impact sensor with two crossed PVDF films was designed and investigated. This sensor has two orthogonal layers of sensing elements that both respond to impacts, which creates positioning information for the impacts. Because of the sensor's structure, a signal processing method was designed based on multisensor fusion theory. Tests were performed to verify the performance of the proposed impact sensor. The average signal-to-noise ratios (SNRs) for impacted PVDF films were 34.79 and 20.23 dB, respectively, for the upper and lower layers, while the average signal-to-clutter ratios (SCRs) for nonimpacted films were 21.90 and 10.05 dB, respectively. The sensor also has an extremely high detection efficiency of at least 1528 collisions per second and can identify particles that impact at the same time.*

Keywords. *Grain loss detection, Impact sensors, Multisensor fusion, Particle impact tests, PVDF films.*

Harvesting machines, such as combines, play an important role in modern agricultural production. However, grain losses are inevitable in the harvesting process, which consists of cutting, threshing, separating, cleaning, and storing. To detect grain losses, impact sensors are usually installed under the separating rotor (Liang et al., 2015a) and behind the cleaning sieve (Xu et al., 2019). These impact sensors count the threshed and unseparated grains of the crop. The number and position of impact sensors depend on a mathematical model of grain threshing and separation. The grain loss ratio can then be calculated based on the number of grains counted by the sensors, the mathematical model, and the combine throughput. Several researchers have developed mathematical models of grain threshing and separation, such as Maertens et al. (2001a, 2001b), Miu et al. (2008a, 2008b), and Tang et al. (2012). Thus, this article focuses on the impact sensors.

To improve the accuracy of grain loss detection, many researchers have engaged in the development of impact sensors. Currently, piezoelectric impact sensors, the detecting surface of which is provided by piezoelectric media, have replaced other types of sensors, such as electromechanical, acoustic, microwave, and machine vision. When grains and material other than grain collide with the piezoelectric media, corresponding electrical signals are generated. Thus, we can distinguish the grains from other material after the raw electrical signals are processed, e.g., by amplification, filtration, wave rectification, envelope detection, etc. A typical impact sensor is composed of a flat impact plate, generally rectangular, and a sensing element, such as a piece of piezoelectric ceramic, that is attached to the rear side of the impact plate. Grains collide with the front side of the impact plate, causing the impact plate to flex. A typical example is the impact sensor presented by Mostofi Sarkari et al. (2007). Ni et al. (2010) arranged multiple impact plates in an array to improve the efficiency and accuracy. Liang et al. (2015b) developed a reformative sensor by pasting a viscoelastic layer in an optimal position to increase the detection speed of the sensor.

Submitted for review in April 2019 as manuscript number ITSC 13440; approved for publication as a Research Article by the Information Technology, Sensors, & Control Systems Community of ASABE in August 2019.

The authors are **Ying Sun,** Doctoral Student, **Rui Cao,** Graduate Student, **Zhan Lu,** Doctoral Student, and **Xin Nie,** Graduate Student, College of Biosystems Engineering and Food Science, Zhejiang University, Hangzhou, China; **Zhaokai Li,** Doctoral Student, College of Electrical Engineering, Zhejiang University, Hangzhou, China; **Yonghua Yu,** Lecturer, **Hongping Tian,** Lecturer, **Xiangqun Qian,** Lecturer, and **Jianping Wang,** Professor, College of Biosystems Engineering and Food Science, Zhejiang University, Hangzhou, China. **Corresponding author:** Jianping Wang, 866 Yuhangtang Road, Hangzhou 310058, China; phone: +86-571-88982350; e-mail: jpwang@zju.edu.cn.

Vol. 62(5): 1195-1205 ISSN 2151-0032 https://doi.org/10.13031/trans.13440

Xu and Li (2009a) explored a new method that was expected to further enhance the performance of impact sensors. They introduced polyvinylidene fluoride (PVDF) films as sensing elements to replace the impact plates and piezoelectric media. PVDF films are superior in that they reduce the sensitivity unevenness and metal vibration noises that are characteristic of traditional sensors. PVDF has many advantages, such as high sensitivity to weak impacts, chemical stability, and flexibility. In addition, PVDF films can be produced in slim, soft, and complex shapes and can withstand repeated collisions when covered with a protective layer, such as polyethylene terephthalate (PET) or silicone rubber. Zhao et al. (2012) upgraded a PVDF sensor with a floating raft damping structure to decrease the amplitude and frequency of vibration interference. However, PVDF sensors are still in the laboratory and are far from actual applications. They need continued development, especially for situations in which the impact signals overlap due to dense and concurrent collisions.

This article presents a novel impact sensor using two crossed PVDF films, which are intended to improve the detection efficiency and accuracy of the sensor. The theory for this novel sensor is that stress and deformation can pass easily between the thin, soft films. Both layers of sensing elements can respond to one collision, for which the position can then be determined. Accordingly, a signal processing method based on multisensor fusion theory is proposed. To measure the performance of the impact sensor and verify its function, collision tests were conducted using a two-particle drop test bench with variable falling heights and positions. Through single, continuous, and two simultaneous collision tests, the sensor's characteristics were studied, including the signal-to-noise ratio (SNR), the signal-to-clutter ratio (SCR), the efficiency, and the relationship between the signals from the two layers. The impact sensor with two crossed PVDF films could obtain the spatial distribution of grain collisions and distinguish between simultaneous collisions.

THEORY

A diagram of the impact sensor with two crossed PVDF films is shown in figure 1. The main body of the sensor consists of a layer of PVDF films aligned in the *x*-direction, a layer of PVDF films aligned in the *y*-direction, a damping layer, and a support plate. The signal processing hardware includes two groups of signal processing devices (one group for each layer of films), two signal collectors (for the *x* and *y* directions), and a computer. The two layers of PVDF films are perpendicular, and the PVDF films within each layer are independent and parallel. Each PVDF film has its own signal processing device, including a charge amplifier, a bandpass filter, an envelope detector, and a voltage comparator. The signals from each layer are combined in a signal collector and are transmitted to the computer after attaching position information. Finally, all the signals are combined in a software program for further processing.

Compared with traditional sensors, this sensor with two layers of sensing elements can provide more impact information. When an impact occurs on its surface, the sensor generates two signals, corresponding to the upper and lower layers. These two signals are distinguished by their response time, amplitude, and frequency, and these parameters are the key to associating the two signals from the two layers. In the sensor, each impact is associated with its position on the sensing elements, meaning that a coordinate is marked in each direction (*x* and *y*). The signal collector then attaches the corresponding time stamp. When the signal, with time and position information, is received by the computer, it can be easily identified.

In most cases, the sensor can also differentiate between two simultaneous impacts. If the impact positions of two grains are not the same in the two directions, the four signals from the four impacted films in the two layers can be combined into two groups according to their characteristics (i.e., their relationships in amplitude or frequency). If two grains hit the same film in one layer, as shown in figure 2 with two grains colliding at the same *x*-position at the same time, then only one signal is generated by the film in the *x*-direction, and two signals are generated by the two films in the *y*-direction in the other layer. Through a series of conditioning processes, such as matching and de-replicating, these three signals can be divided into two groups, and the two collisions can be distinguished. Conversely, if two particles impact the same film in the *y*-direction, the above method works the same way. There is only one situation in which two particles cannot be distinguished, and that is if they impact at the same position at the same time. Thus, the impact sensor using two crossed PVDF films can increase the grain loss detection accuracy.

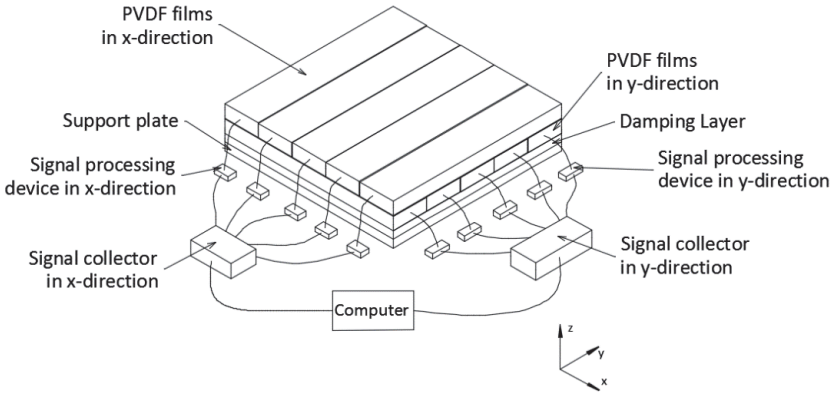

Figure 1. Structure of impact sensor with two crossed layers of PVDF films.

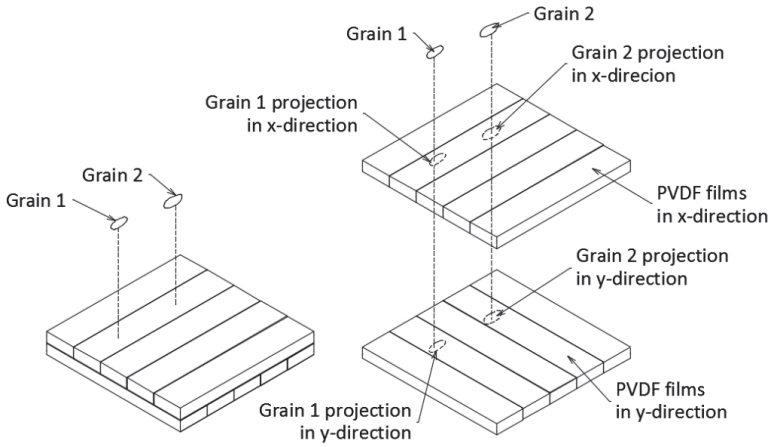

Figure 2. Two grains simultaneous impacting on the same film in the *x*-direction but on different films in the *y*-direction.

MATERIALS AND METHODS

SENSOR DEVELOPMENT

The PVDF films used in this sensor were already polarized, protected by PET films, and connected to leads. These films were produced by Measurement Specialties (Fairfield, N.J.) and had a mechanoelectrical conversion of 0.4 V μm^{-1}. The length, width, and thickness of the PVDF films were 170 mm, 21 mm, and 0.228 mm, respectively (including a PVDF layer of 28 μm thickness and two protective PET layers of 0.2 mm thickness). Before installing the PVDF films, their characteristic parameters were tested with an LCR meter (IM3533-01, Hioki Corp., Nagano, Japan). The tested parameters included capacitance, resistance, and inductance, and their overall variations in the twelve PVDF films were 3.69%, 0.82%, and 2.76% respectively.

The proposed sensor with two crossed layers of PVDF films is shown in figure 3. The dimensions of the main body are 200 mm × 200 mm × 8 mm (L × W × H). The bottom shell can be fixed on a plate or a bracket, and the top shell can be mounted on the bottom shell with screws. Both shells were made of 304 stainless steel, which fully meets the requirements of static and impact strength for collisions. Between the two shells are four layers from bottom to top: a damping layer, two layers of PVDF films, and a nonslip sheet. The damping layer was smoothly pasted onto the bottom shell. We used silicone rubber as the damping layer because of its stability and elasticity. The two layers of PVDF films were pasted onto the surface of the damping layer. The upper layer was in the *x*-direction, and the lower layer was in the *y*-direction. There were six PVDF films in each layer. The width of each film was 21 mm, and the spacing between adjacent films was 0.8 mm. Therefore, the effective sensing area of the sensor was 130 mm × 130 mm. The nonslip sheet pasted under the top shell was a hollow square of thin silicone rubber that pressed the PVDF films tightly. The leads of the PVDF films were connected to the charge amplifiers of the signal processing devices via adapter plates.

TEST BENCH

To study the performance of the sensor, we designed a test bench that dropped two particles with variable coordinates in the *x*, *y*, and *z* directions, as shown in figure 4a. Five sliding mechanisms determine the two drop locations, the largest of which is the drop height adjustment. The range of drop height (the *z*-direction) is 280 to 700 mm, and the speed at which the grains impact the sensor is 2.34 to 3.70 m s^{-1},

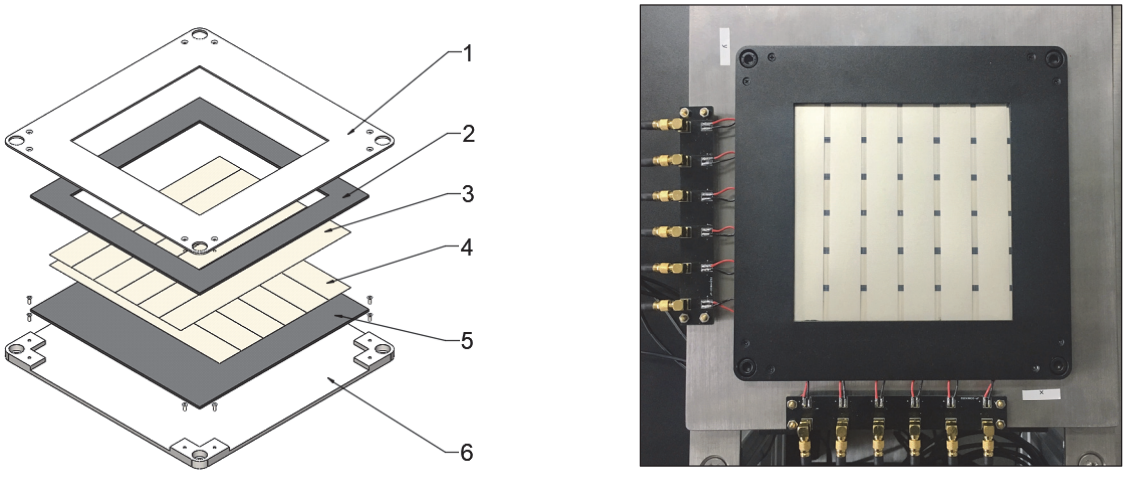

(a) **(b)**

Figure 3. (a) Structure and (b) photo of impact sensor: 1 = top shell, 2 = nonslip sheet, 3 = PVDF films in the *x*-direction, 4 = PVDF films in the *y*-direction, 5 = damping layer, and 6 = bottom shell.

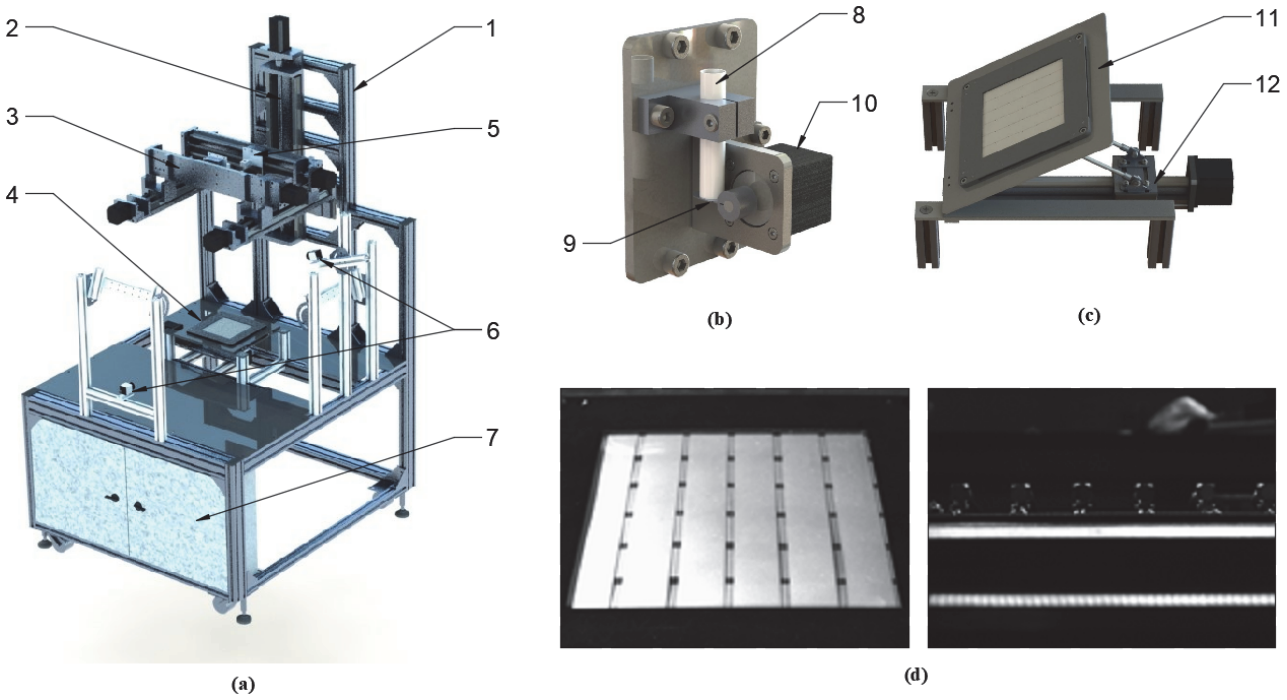

Figure 4. (a) Collision test bench: 1 = support, 2 = height adjustment mechanism, 3 = position adjustment mechanism, 4 = angle adjustment mechanism, 5 = release mechanism, 6 = high-speed cameras, 7 = control cabinet; (b) release mechanism: 8 = tube, 9 = cover, 10 = motor; (c) angle adjustment mechanism: 11 = plate, 12 = slide; and (d) views of the two cameras.

which matches the best range for impact sensor installation reported by Tang et al. (2012). The position adjustment consists of the other four sliding mechanisms, and the range in the *x* and *y* directions is 200 mm × 200 mm. Two release mechanisms are located on the sliders of the position adjustment mechanism. These release mechanisms, shown in figure 4b, are triggered by motors. After a particle is placed in the tube, the motor rotates the cover, and the particle drops by gravity and hits the sensor below. An angle adjustment mechanism is used to change the angle of the sensor from 0° to 70°, as shown in figure 4c. The sensor is fixed on a plate and rotated by a slide. In this study, we set the angle to 0° to study the sensor's performance with vertical impacts. We also used two high-speed cameras (MARS 640-815 µm, Vision Datum Co., Hangzhou, China) to monitor the impact positions and calculate the difference in impact time of the particles. The views of the two cameras are shown in figure 4d.

Control and Signal Acquisition

The test bench control and the signal acquisition system are shown in figure 5. The core of the system is a software program designed in LabVIEW (v2015, National Instruments, Austin, Tex.). The main functions of the software are sending instructions to the microcontroller and saving the signals from the twelve PVDF films. In the software, channels 1 to 6 correspond to films X1 to X6, respectively, and channels 7 to 12 correspond to films Y1 to Y6. In the test bench, five motors control the sliding mechanisms, and two motors control the release mechanisms. We used a STM8S105 microcontroller to control the motor drivers and proximity switches for limiting movements of the sliding mechanisms. When a collision occurs on the surface of the sensor, electric charges are produced by the impacted PVDF films. We used two multichannel charge amplifiers (CT5853, Chengtec Electronics Co., Ltd., Shanghai, China) to convert these electric charges to voltage signals. These signals are then transmitted to the computer through a data

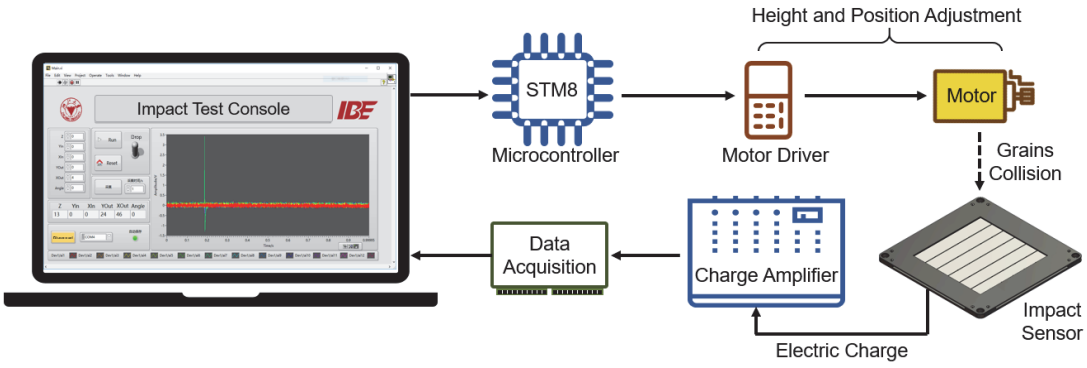

Figure 5. Test bench control and signal acquisition system.

acquisition device (USB-6210, National Instruments, Austin, Tex.) and used in the software.

Collision Tests

To measure the sensor's performance, we performed full-factorial collision tests using the impact position and drop height as variables. We chose regular spheres made of acrylonitrile butadiene styrene (ABS) as the impacting objects, mainly to avoid the experimental uncertainty caused by the irregular shapes of grains. The ABS balls had a diameter of 4 mm, a density of 1020 kg m^{-3}, a mass of 34.2 mg, an elastic modulus of 200 MPa, and a Poisson's ratio of 0.39. These parameters are similar to those of grain (Xu and Li, 2009b). The ABS balls used in the experiments and typical rice grains are shown in figure 6.

The effective sensing area can be divided into 36 double-layered squares. We marked the center of every square and used these points as the centers of circles with a radius of 4 mm, which matches the inside diameter of the tubes in the release mechanisms. These circles were the impact positions. According to the coordinates on the sensor, every impact position was denoted as P_{XnYm} (n = 1, 2, ..., 6; m = 1, 2, ..., 6). The particle drop height (H_i, i = 1, 2, …, 7) was set to seven levels: 700, 630, 560, 490, 420, 350, and 280 mm. We repeated the impact test three times at every position and every height.

After these full-factorial collision tests, we performed a continuous collision test and a simultaneous collision test to verify the performance of the sensor. In the continuous collision test, ten particles were released to impact the sensor at random times, heights, and positions, with the two high-speed cameras recording the process. In the simultaneous collision test, two particles impacted on the sensor simultaneously, and the process was recorded. These two collision tests were used to verify if the sensor could identify and count multiple particles.

(a) (b)

Figure 6. (a) ABS balls used in experiments and (b) rice grains.

Signal Feature Extraction

A group of typical collision signals (for height H_4 and position P_{X3Y3}) from the sensor is shown in figure 7a. Among the signals for all twelve channels, the two most significant

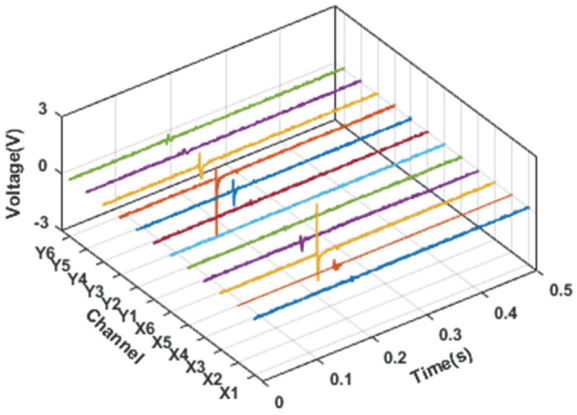

(a)

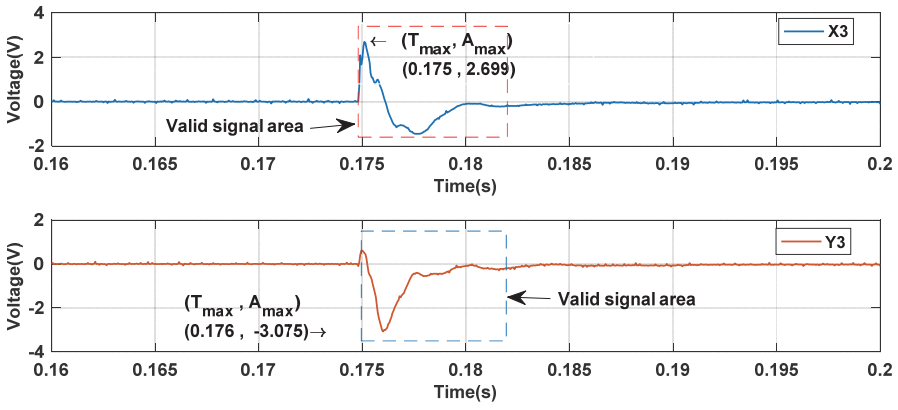

(b)

Figure 7. (a) Typical collision signals from twelve channels and (b) feature extraction for height H_4 and location P_{X3Y3}.

peaks come from the collision position. Other channels also have signals whose peaks decrease as the distance from the collision position increases, mainly because of vibration transmission. Signals from nonimpacted channels disturb the identification of the collision signals; this clutter should be suppressed for sensor optimization. Extraction of the signals of the impacted channels is shown in figure 7b. The three features of a signal are the absolute maximum amplitude (A_{max}), the time of absolute maximum amplitude (T_{max}), and the response duration (T_{dur}). In particular, we defined ±0.2 V as the boundaries of a valid signal area because the maximum noise in a no-load signal is 0.133 V, and a signal can be clearly distinguished when it is 1.5 times greater than the noise. The valid signal area begins when A_{max} is >0.2 V and ends when A_{max} is <0.2 V in the next ten points. In this way, only the information of the first collision is extracted as the signal feature, even if there are multiple collisions due to rebounding of a particle.

Signal Processing

Unlike single-layer sensors, two-layer sensors cannot calculate the number of collisions by their summation because a single collision on the two-layer sensor will generate two signals on the upper and lower sensing elements. Therefore, the first step in counting the collisions is to identify whether the signals from the two layers come from the same collision. Combining the signals of multiple sensing elements and extracting their features is a signal processing method called multisensor fusion. Considering the multiple impacts on the sensor, we need to determine if there are simultaneous collisions before we can calculate the number of collisions. The data fusion architecture for counting and identifying collisions within a period of time is shown in figure 8. First, for the extracted features from the twelve channels for both layers, *M* and *N* are the numbers of channels with collision signals, X*i* and Y*j* are their serial numbers (multiples of each, possibly), and X*i*-A_{max}, X*i*-T_{max}, Y*j*-A_{max}, and Y*j*-T_{max} are their absolute maximum amplitudes and corresponding times, respectively. For groups X*i* and Y*j* according to the time dimension, the following is true: when the difference in their T_{max} values is less than a certain value, they can be considered to be one collision or simultaneous collisions. When a simultaneous collision occurs, an amplitude relationship model is needed to assess the impact positions. Finally, for the output of the number and position of the collisions, the larger value of *M* and *N* [max(*M*, *N*)] is the number of collisions, and (X*i*, Y*j*) is the position.

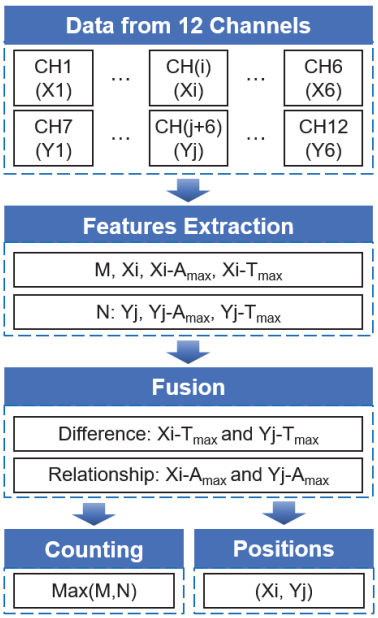

Figure 8. Data fusion architecture for counting and identifying collisions in a period of time.

Results and Discussion

Sensor Signal-to-Noise Ratio

The SNR is the ratio of the signal power to the background noise power. It is used to assess the significance of signals. It can be calculated by the amplitudes of the signal (A_{signal}) and noise (A_{noise}) using the following equation:

$$SNR\ (dB) = 20 \log_{10}\left(\frac{A_{signal}}{A_{noise}}\right) \quad (1)$$

Figure 8 shows the SNR values for all positions using a drop height of 630 mm (H_2). The SNRs for the upper layer are generally higher than those for the lower layer. For the upper layer, the average SNR is 34.79 dB, the minimum SNR is 24.33 dB (at P_{X6Y4}), and the maximum SNR is 40.62 dB (at P_{X2Y4}). For the lower layer, these values are 20.23 dB, 5.76 dB (at P_{X6Y6}), and 35.51 dB (at P_{X3Y2}), respectively. When using ±0.2 V (3.52 dB in SNR) as the boundary of the valid signal area, all positions in the upper and lower layers produced notable signals at a drop height of 630 mm (H_2). However, for particles dropped from other heights, especially the lower heights such as 280 mm (H_7) and 350 mm (H_6), the proportions of positions that produced valid signals were 94.4% and 93.1%, respectively.

The SNR needs to be improved, especially for the lower layer. Placing the two layers of PVDF films closer together or improving the sensitivity of the lower layer are feasible ways to improve the SNR. Moreover, this sensor was handmade due to laboratory limitations. This led to poor bonding due to low pressure on the PVDF films; as a result, the sensitivities at different positions on the sensor were quite different, which can be seen in figure 9. The SNRs of the lower layer at some positions (P_{X3Y2} and P_{X3Y3}) were very close to those of the upper layer. This suggests that, with high-quality production, both layers of the sensor can have great sensitivity.

Sensor Signal-to-Clutter Ratio

All impact sensor arrays have the same problem, which is that the nonimpacted sensing elements have clutter noise due to vibration transmission. The SCR is used to measure the interaction between sensing elements. The equation for SCR is the same as the equation for SNR. We used the impacted films and four nonimpacted films (two adjacent films on the left and right, if any) to investigate the SCR of the sensor. Figure 10 shows the signal amplitudes for the twelve impacted films and their four adjacent films in the upper and lower layers for height H_2. The twelve collision positions

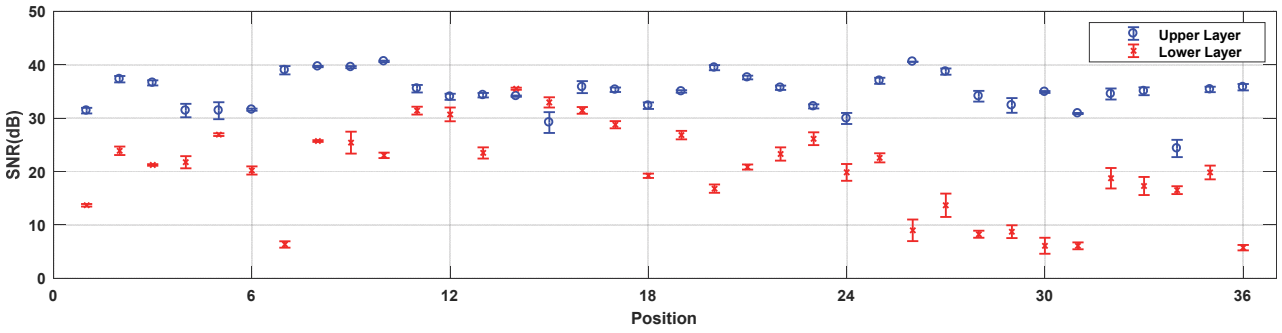

Figure 9. SNR values of upper and lower layers at each position for a drop height of 630 mm (H_2).

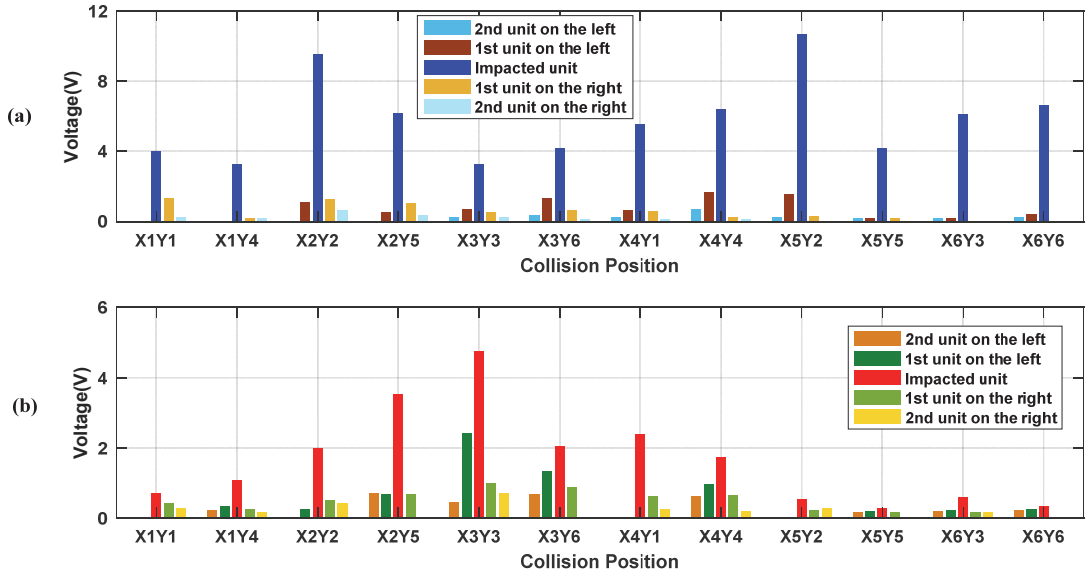

Figure 10. Signal amplitudes for impacts on twelve films and their adjacent four films in the (a) upper and (b) lower layers for height H_2.

were selected uniformly. In general, the SCR of the upper layer is greater than that of the lower layer. For the upper layer, the average SCR of the adjacent sensing elements is 21.90 dB, and the SCR of every other sensing element is 26.88 dB; these values are 10.05 and 13.77 dB, respectively, for the lower layer. The structure of the two crossed PVDF films creates interference in the impact vibrations, which is disadvantageous for identifying and counting collisions. It is necessary to reduce the SCR in further studies.

Sensor Efficiency

Detection efficiency is the maximum number of collisions that can be detected per unit time, which is an important indicator of sensor performance. Efficiency is related to the duration of the collision responses. Figure 11 shows the T_{dur} values for twelve positions in the upper and lower layers. For the upper layer, the average, longest, and shortest T_{dur} were 0.0089 s, 0.0157 s (at P_{X2Y2}) and 0.0043 s (at P_{X6Y6}), respectively. For the lower layer, these three values were 0.0052 s, 0.0004 s (at P_{X1Y1}) and 0.0116 s (at P_{X2Y2}), respectively. The T_{dur} becomes longer as the peak amplitude increases, so the longest T_{dur} is used to calculate the efficiency. When T_{dur} is 0.0157 s, the number of detectable collisions per second per position is 63.7, and this sensor with twelve sensing elements could detect 1528.8 collisions per second. We used ±0.2 as the boundary of the effective area in this study; when grains and other material are distinguished by the signal amplitude, the boundary should be in-

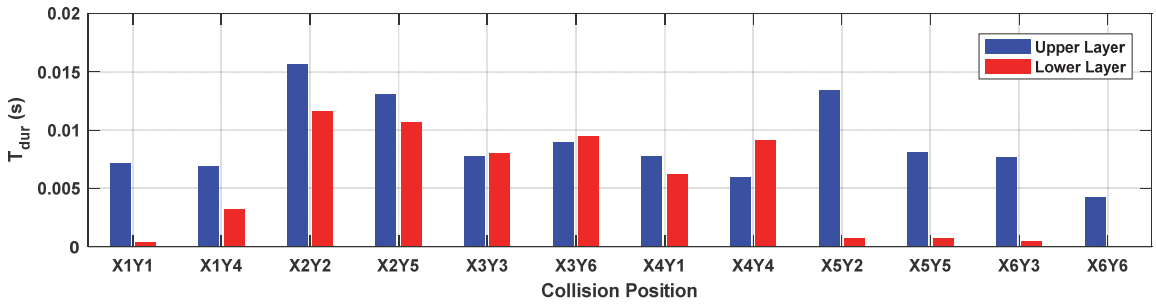

Figure 11. Response duration (T_{dur}) at twelve positions in the upper and lower layers for height H_2.

creased, and T_{dur} will be reduced. Therefore, the actual efficiency of the sensor will be greater than this calculated value.

Relationship between Sensor Layers

The relationship between the signals acquired from the two layers is the key to determining whether the signals correspond to a single collision.

Response Time

The T_{max} values of the collision signals for every height (except collisions whose A_{max} was less than ±0.2 V) are shown in figure 12. The maximum difference in T_{max} between the two layers is 3.7×10^{-3} s, and the minimum difference is 0 s. These data show that the responses of the two layers are almost synchronous. In other words, if the two layers' signals result from the same collision, then the difference between their T_{max} values should be no more than 3.7×10^{-3} s.

Response Amplitude

Under ideal conditions, the two layers of PVDF films would be close and their motions would be synchronized; therefore, their response amplitudes should be almost identical. However, the handmade sensor had gaps between the layers that caused the films to bend; this curvature increased the sensitivity of the films. Clearly, making sensors with soft, slim PVDF films puts higher demands on the manufacturing process, especially for a sensor with two layers of PVDF films. Because of the rebounding of particles, the response amplitude does not have a linear relationship with height. However, for different heights, the distribution of measurements at each position on the surface of the sensor was consistent. Tests were performed at every height and position to build an A_{max} model for comparison of the collision signals. Figure 13 shows the distributions of A_{max} values at each position in the upper and lower layers for height H_2.

Verification of Tests Results

Continuous Collision Test

The signals from the twelve channels were combined in the continuous collision test, as shown in figure 14. There were eleven highly significant peaks whose A_{max} was >1 V, five smaller peaks whose A_{max} was between 0.2 and 1 V, and three basic noises (CH1, CH2, and CH6) that drifted at a considerable scale. Corresponding to the collision process captured with the high-speed cameras, these 16 peaks were caused by ten particles' impacts or their secondary impacts due to rebounding after the first impact, and the basic noise drift was due to the particles rolling on the PVDF films. The sensor exactly reflected the action of the particles in real time. When particles impacted the sensor one by one, each collision was recorded as a single collision with a time parameter, and the sensor easily recognized and counted the impacts. Secondary collisions and basic noise drifts are the main problems in this case. These problems can be solved by setting the sensor at an appropriate angle, which would cause particles to bounce off the surface of the sensor after colliding.

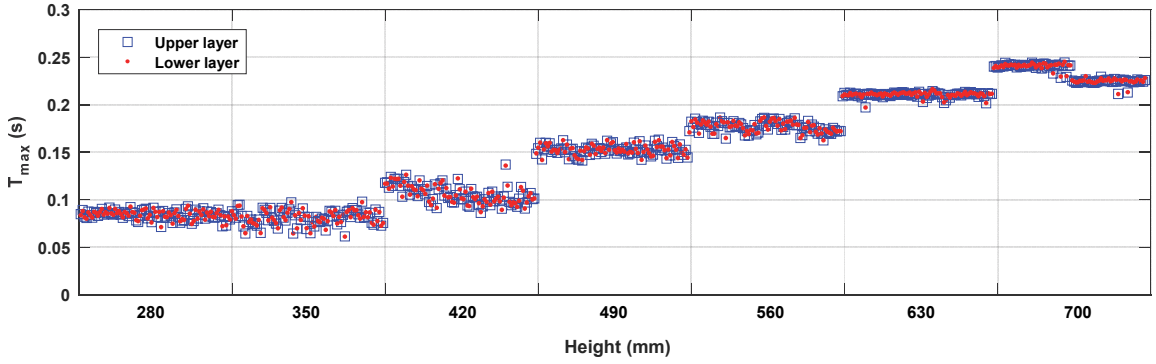

Figure 12. Time of absolute maximum amplitude (T_{max}) of collision signals for every height.

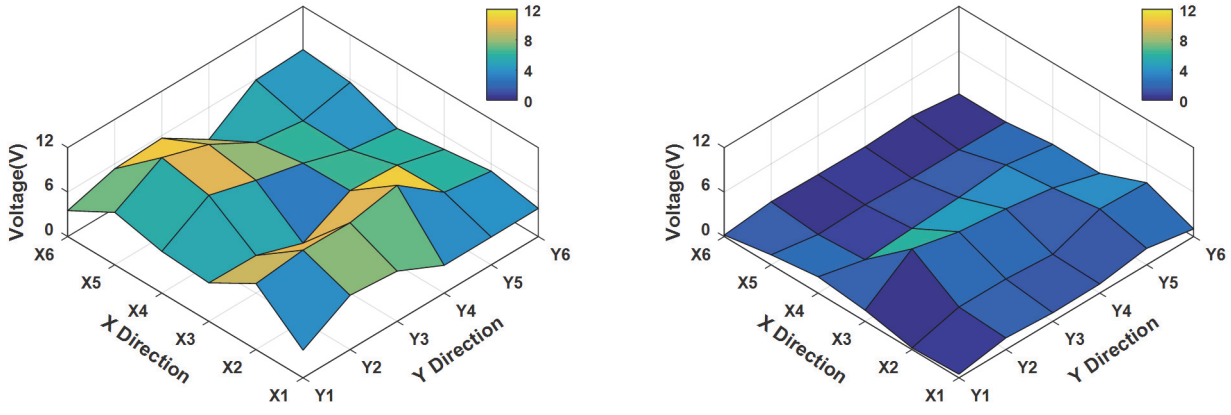

Figure 13. Absolute maximum amplitude (A_{max}) in the (a) upper and (b) lower layers at each position for height H_2.

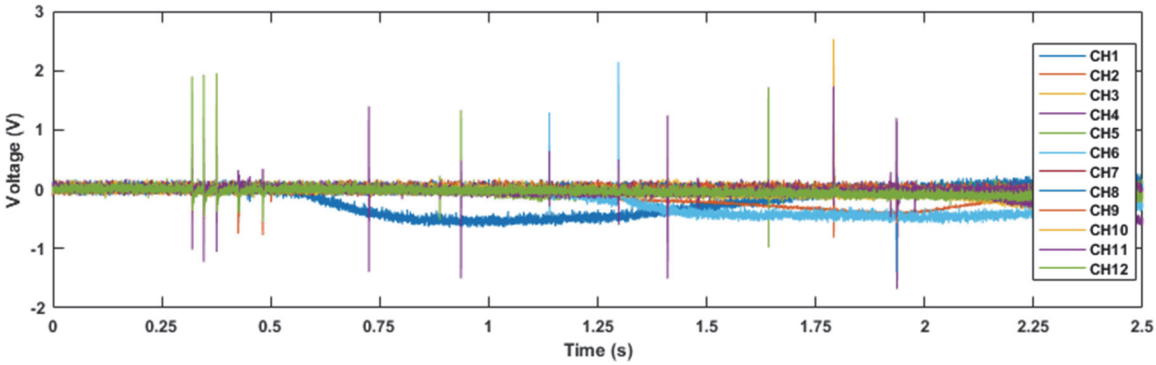

Figure 14. Signals from twelve channels in the continuous collision test.

Simultaneous Collision Test

The signals from the twelve channels were combined in the simultaneous collision test, in which two particles simultaneously collided at two different positions, as shown in figure 15a. There was a group of significant signals at 0.25 s, and smaller peaks at 0.43 s were caused by the particles rebounding. Extracting the four signals with significant peaks, as shown in figure 15b, resulted in four coordinates: X3

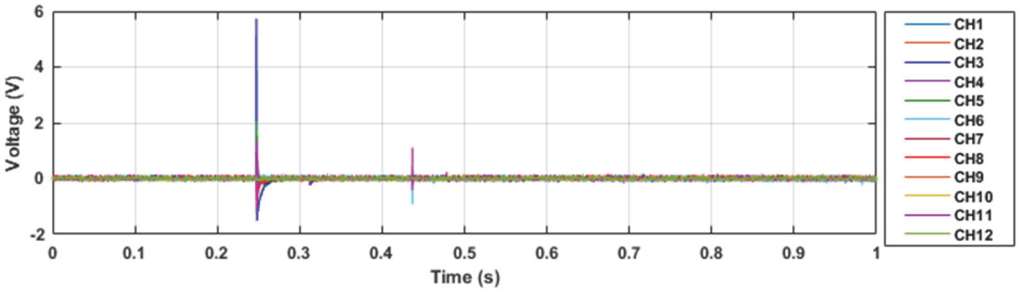

(a)

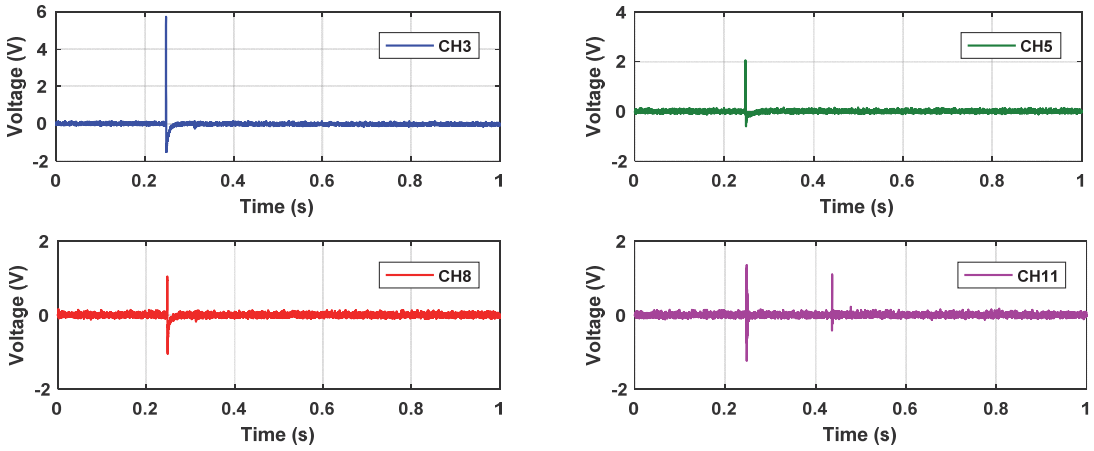

(b)

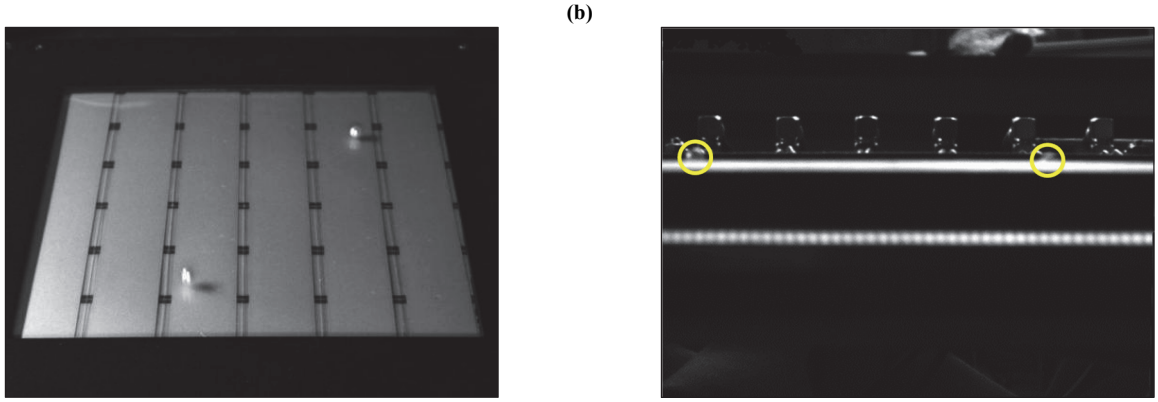

(c)

Figure 15. (a) Signals from twelve channels, (b) channels with significant peaks, and (c) particles colliding simultaneously at two positions.

(CH3), X5 (CH5), Y2 (CH8), and Y5 (CH11). These coordinates correspond to two possible combinations of the collision positions: P_{X3Y2} and P_{X5Y5}, or P_{X3Y5} and P_{X5Y2}. In the previous test, we recorded the signals at 36 positions and seven heights, so we can assess these positions by comparing them to the previous data. The collision positions were P_{X3Y2} and P_{X5Y5}, and the moment of collision is shown in figure 15c.

For two particles colliding on one PVDF film, the signals from the twelve channels are shown in figure 16a. Ignoring the secondary impacts at 0.37 s and 0.43 s, there were significant peaks at 0.25 s. Three signals with significant peaks from CH3, CH5, and CH11 (X3, X5, and Y5) are shown in figure 16b. When two signals come from the same layer, we know that two particles are impacting on the sensor, and the collision positions are P_{X3Y5} and P_{X5Y5}. The moment of collision, as captured by the high-speed cameras, is shown in figure 16c.

Conclusions

A novel impact sensor using two crossed polyvinylidene fluoride (PVDF) films as sensing elements was designed and examined to improve the accuracy and efficiency of collision detection. The sensing elements in two orthogonal layers could obtain the coordinates of the impacts and thereby distinguish simultaneous impacts at different locations.

The single-collision experiment showed that the average signal-to-noise ratios (SNRs) were 34.79 and 20.23 dB for the upper and lower layers, respectively. The signals were generally smaller from the lower layer than the upper layer, which was due to the distance between the sensing surfaces of the PVDF film layers. Nonimpacted PVDF films could also be affected by collisions on a nearby film. For the upper layer, the average signal-to-clutter ratio (SCR) of adjacent sensing elements was 21.90 dB, and the SCR of every other sensing element was 26.88 dB; these two values were 10.05

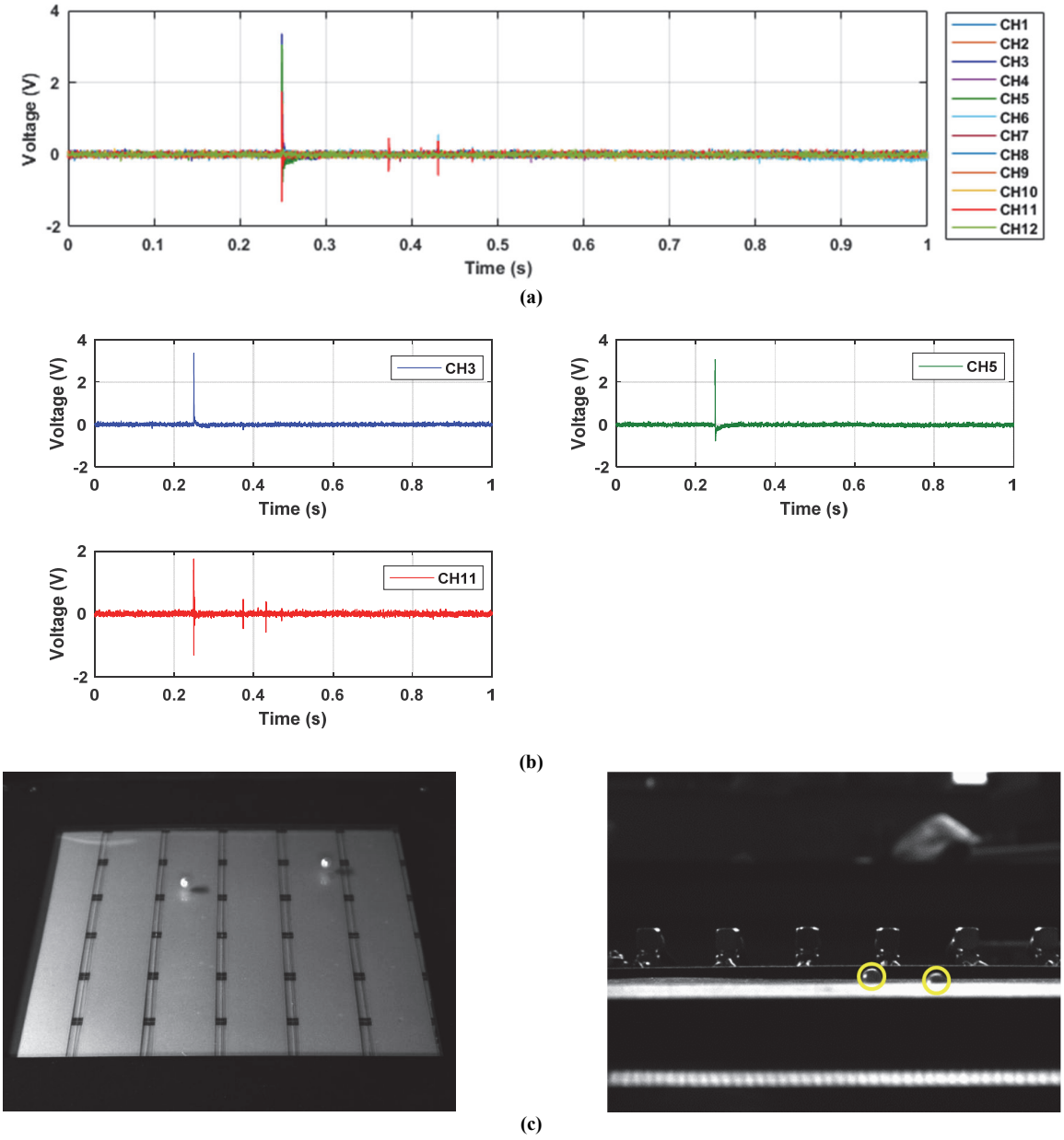

Figure 16. (a) Signals from twelve channels, (b) channels with significant peaks, and (c) particles colliding simultaneously on one film.

and 13.77 dB, respectively, for the lower layer. Regarding the efficiency of the sensor, the minimum number of collisions that the sensor was able to detect was 1528.8 per second. For impacts from different drop heights, the difference in T_{max} between the two layers was no more than 3.7×10^{-3} s. The continuous collision test confirmed that the sensor could easily recognize and count every impact, and the simultaneous collision test indicated that the sensor could distinguish two particles impacting at the same time.

The tests verified the feasibility of this novel impact sensor based on two crossed PVDF films. Future studies will focus on optimizing the uniformity, SNR, and SCR of the sensor so that a surface model of the response can be established. In addition, integration and protection of the sensor are necessary to meet the complex working conditions in field applications.

ACKNOWLEDGEMENTS

The authors gratefully acknowledge financial support provided by the National Key Technologies R&D Program of China (Grant No. 2016YFD0700105).

REFERENCES

Liang, Z., Li, Y., Zhao, Z., & Xu, L. (2015a). Structure optimization of a grain impact piezoelectric sensor and its application for monitoring separation losses on tangential-axial combine harvesters. *Sensors, 15*(1), 1496-1517. https://doi.org/10.3390/s150101496

Liang, Z., Li, Y., Zhao, Z., Xu, L., & Li, Y. (2015b). Optimum design of grain sieve losses monitoring sensor utilizing partial constrained viscoelastic layer damping (PCLD) treatment. *Sensors Actuators A, 233*, 71-82. https://doi.org/10.1016/j.sna.2015.06.010

Maertens, K., De Baerdemaeker, J., Ramon, H., & De Keyser, R. (2001a). Power and machinery: An analytical grain flow model for a combine harvester, Part I: Design of the model. *J. Agric. Eng. Res., 79*(1), 55-63. https://doi.org/10.1006/jaer.2000.0679

Maertens, K., De Baerdemaeker, J., Ramon, H., & De Keyser, R. (2001b). Precision agriculture: An analytical grain flow model for a combine harvester, Part II: Analysis and application of the model. *J. Agric. Eng. Res., 79*(2), 187-193. https://doi.org/10.1006/jaer.2000.0681

Miu, P. I., & Kutzbach, H.-D. (2008a). Modeling and simulation of grain threshing and separation in axial threshing units: Part II. Application to tangential feeding. *Comput. Electron. Agric., 60*(1), 105-109. https://doi.org/10.1016/j.compag.2007.07.004

Miu, P. I., & Kutzbach, H.-D. (2008b). Modeling and simulation of grain threshing and separation in threshing units: Part I. *Comput. Electron. Agric., 60*(1), 96-104. https://doi.org/10.1016/j.compag.2007.07.003

Mostofi Sarkari, M. R., Jamshidi, B., & Minaei, S. (2007). Field evaluation of grain loss monitor in different harvesting condition on combine JD-955. *Proc. 10th Intl. Congress Mech. Energy Agric.* Rome, Italy: AGRIS.

Ni, J., Mao, H., & Li, P. (2010). Design of intelligent grain cleaning losses monitor based on array piezocrystals [in Chinese]. *Trans. Chinese Soc. Agric. Mach., 41*(8), 175-177. http://doi.org/10.3969/j.issn.1000-1298.2010.08.036

Tang, Z., Li, Y. M., Zhao, Z., Liang, Z. W., & Chen, Y. (2012). Effect of different installed location of entrainment loss sensor on grain testing accuracy [in Chinese]. *Trans. Chinese Soc. Agric. Eng., 28*(10), 46-52. http://doi.org/10.3969/j.issn.1002-6819.2012.10.008

Xu, J. J., & Li, Y. M. (2009a). A PVDF sensor for monitoring grain loss in combine harvester. *Computer and Computing Technologies in Agriculture (CCTA 2009), III* (pp. 499-505). IFIP Advances in Information and Communication Technology, Vol. 317. Berlin, Germany: Springer. https://doi.org/10.1007/978-3-642-12220-0_72

Xu, L. Z., & Li, Y. M. (2009b). Critical speed of impact damage on a rice kernel [in Chinese]. *Trans. Chinese Soc. Agric. Mach., 40*(8), 54-57. http://en.cnki.com.cn/Article_en/CJFDTOTAL-NYJX200908011.htm

Xu, L., Wei, C., Liang, Z., Chai, X., Li, Y., & Liu, Q. (2019). Development of rapeseed cleaning loss monitoring system and experiments in a combine harvester. *Biosyst. Eng., 178*, 118-130. https://doi.org/10.1016/j.biosystemseng.2018.11.001

Zhao, Z., Li, Y., Liang, Z., & Chen, Y. (2012). Optimum design of grain impact sensor utilizing polyvinylidene fluoride films and a floating raft damping structure. *Biosyst. Eng., 112*(3), 227-235. https://doi.org/10.1016/j.biosystemseng.2012.04.005